THE JOURNAL OF PHYSICAL CHEMISTRY A

Article

Properties and Thermal Decomposition of the Hidro-Fluoro-Peroxide CH3OC(O)OOC(O)F

Matias Berasategui, Maximiliano Alberto Burgos Paci, and Gustavo Alejandro Argüello

J. Phys. Chem. A, **Just Accepted Manuscript** • DOI: 10.1021/jp407871x • Publication Date (Web): 18 Feb 2014

Properties and Thermal Decomposition of the Hydro-Fluoro-Peroxide $CH_3OC(O)OOC(O)F$

*Matías Berasategui, Maxi A. Burgos Paci and Gustavo A. Argüello**

Instituto de Investigaciones en Físico Química de Córdoba (INFIQC) CONICET-UNC, Departamento de Físico Química, Facultad de Ciencias Químicas, Universidad Nacional de Córdoba, Ciudad Universitaria, X5000HUA Córdoba Argentina.

KEYWORDS: Peroxides, Gas phase thermal decomposition, Bond dissociation energy.

*Corresponding Author: gaac@fcq.unc.edu.ar

ABSTRACT The thermal decomposition of methyl fluoroformyl peroxycarbonate $CH_3OC(O)OOC(O)F$ was studied in the range of 30 – 96 ºC using FTIR spectroscopy to follow the course of the reaction in the presence of either N_2, O_2, or CO as bath gases. The rate constants of the homogeneous first-order process fit the Arrhenius equation $k_{exp} = (5.4 \pm 0.2) \times 10^{14} \exp[-(27.1 \pm 0.6$ kcal $mol^{-1}/RT)]$ (in units of s^{-1}). A complete mechanism of decomposition is presented. An experimental O-O bond energy of 27 ± 1 kcal mol^{-1} was obtained. The products observed when N_2 or O_2 are used as bath gases were CO_2, CO, HF, and $CH_3OC(O)H$, while in the presence of CO $CH_3OC(O)F$ was also observed. Transition State *ab initio* calculations were carried out to understand the dynamics of the decomposition. Additionally, thermodynamic properties of the atmospherically relevant CH_3OCO_2• radical were calculated. The heat of formation, $\Delta H°_{f\,298}$, obtained for CH_3OCO_2• and $CH_3OC(O)OOC(O)F$ were 78 ± 3 kcal mol^{-1} and 191 ± 5 kcal mol^{-1} respectively.

Introduction

Since the replacement of chlorofluorocarbons (CFCs) by compounds commonly designated as hydrofluorocarbons (HFCs), there have been exhaustive studies of the mechanisms, intermediates, and final products of the degradation reactions.[1] Along with these, in the past decade much work has been devoted to the study of the properties and reactions of many compounds and radicals containing only F, C, and O atoms that can be formed in the laboratory as a result of the degradation of HFCs in the presence of oxygen and high concentrations of CO. The study of these reactions afforded many new compounds to be synthesized and used as precursors of atmospherically relevant radicals which were thus isolated.[2-4] Several such compounds have been known for many years (e.g. $CF_3OC(O)OOCF_3$[5] and FC(O)OOC(O)F[6]), and many others have been discovered and characterized during the last years (e.g. $CF_3OC(O)OOC(O)OCF_3$, $CF_3OC(O)OOOC(O)OCF_3$, $CF_3OC(O)OOC(O)F$, and FC(O)OOOC(O)F). [7-10]

The title compound. methyl fluoroformyl peroxycarbonate ($CH_3OC(O)OOC(O)F$) has been recently isolated for the first time[11] from the reaction of methanol and bis-fluoroformyl peroxide. In that system, $CH_3OC(O)OOC(O)F$ was formed as the first stable intermediate as reaction (1) shows, with a further reaction with methanol to form the fully hydrogenated peroxide (2)

$$FC(O)OOC(O)F + CH_3OH \rightarrow CH_3OC(O)OOC(O)F + HF \quad (1)$$

$$CH_3OC(O)OOC(O)F + CH_3OH \rightarrow CH_3OC(O)OOC(O)OCH_3 + HF \quad (2)$$

$CH_3OC(O)OOC(O)F$ is stable at room temperature and can therefore be isolated, distilled and purified. It is of interest since it couples a fluorinated moiety with a hydrogenated one, whose combined properties could represent a transition from a purely fluorocarbooxygenated molecule to a hydrogenated one.

Kinetic data on gas phase thermal decomposition are needed in order to have reliable estimates of bond energies, to help in the elucidation of mechanisms and in the calculation of thermodynamic properties. Nevertheless, this kind of studies has been reported for just a few fluorocarbooxygenated peroxides and trioxides.[12-14] In the present work, thermal decomposition rate constants have therefore been measured as a function of temperature for $CH_3OC(O)OOC(O)F$ in N_2, O_2 and CO, thus providing new data to add to available databases.

The strength of the O—O bond is of fundamental importance in a variety of chemical processes. A value of 34 kcal mol^{-1} has been ascribed to a generic O—O bond dissociation energy for simple homolytic rupture. However, theoretical calculations of the mechanism of O—O bond cleavages in diacyl peroxides have postulated that they are more complex than a simple homolytic cleavage[15]. The dynamics of dissociation of acyl peroxides is being revisited since papers from the sixties have come under scrutiny. Femtosecond time resolution spectroscopy is affording new insights into these reactions and providing data on decarboxylation of carboxyl radicals[16-19].

We also present theoretical calculations of the heat of formation as well as a comprehensive study of all probable transition states involved in the decomposition of $CH_3OC(O)O$-$OC(O)F$, using a variety of methods such as the second-order Möller-Plesset perturbation theory (MP2) associated to the 6-31+G* basis set, the Becke´s three parameter hybrid functional method using the Lee-Yang-Parr correlation functional (B3LYP) associated to the 6-311++G** basis set and the composite method Gaussian-2 (G2).

The CH_3OCO_2• radical is a primary dissociation product of this peroxide, about which very little is known. We contribute a theoretical study about this important and elusive radical with the purpose of deriving some properties such as its structural parameters, vibrational spectrum, and heat of formation.

Experimental section

Caution**!** Although this study was conducted without mishap, it is important to take appropriate safety precautions when manipulating peroxyfluorinated compounds. Reactions involving these substances should be carried out only in millimolar quantities.

General Procedures and Reagents. Volatile materials were manipulated in a glass vacuum line equipped with two capacitance pressure gauges (0-760 Torr, MKS Baratron; 0-70 mbar, Bell and Howell), three U traps, and valves with poly(tetrafluoroethylene) stems (Young, London). For the synthesis of $CH_3OC(O)OOC(O)F$ a stainless steel reactor was connected in parallel to a double-jacket stainless steel IR gas cell (optical path length 200 mm, KBr or Sapphire interchangeable windows) and to the vacuum line. The IR cell was placed in the sample compartment of a Fourier transform infrared instrument (Bruker IFS28). The cell and the reactor were connected by a PTFE pipe using Swagelok valves and connectors. This arrangement made it possible to follow either the course of the synthesis, purification processes, or the thermal decay of substances.

Only a brief description of $CH_3OC(O)OOC(O)F$ synthesis will be given here since it has previously been reported[11]. The reaction was carried out at room temperature, and the reactor was typically loaded with CH_3OH and excess $FC(O)OOC(O)F$. The reaction stopped when CH_3OH was consumed (about 30 minutes), and $CH_3OC(O)OOC(O)F$ was distilled in-situ, i.e. by immersion of the whole reactor in ethanol baths at -100 and -60 ºC to carefully remove excess of $FC(O)OOC(O)F$ and by-products. Immediately after, the double-walled IR cell was loaded with pure $CH_3OC(O)OOC(O)F$ to study the thermal decomposition in the sample compartment of the spectrometer. The outer jacket of the cell was connected to a thermostat, from which hot water flowed at temperatures ranging between 25 and 100 °C with an uncertainty of ± 0.5 °C. Once the cell reached the selected temperature, 2-3 mbar of $CH_3OC(O)OOC(O)F$ was admitted and the pressure was immediately increased to 700 mbar with

either N_2, O_2 or CO. A series of in situ timely spaced IR spectra was obtained. As the absorption bands of the products and $CH_3OC(O)OOC(O)F$ do not overlap in the C=O stretching region, no further treatment was required, and the data processing of the kinetic measurements was done using the absorption bands of the peroxide at 1834 and 1907 cm^{-1}. Most of the products obtained (CO_2, CO, $CH_3OC(O)H$, HF, etc.) were identified from reference spectra of pure samples.

Chemicals. Bath gases were obtained from commercial sources at the following purities: N_2 (>99.9%) and O_2 (>99.9%), CO (>99%). Methanol was analytic grade and used without further purification, and FC(O)OOC(O)F was taken from our own repository samples.

Instrumentation. (a) Vibrational Spectroscopy. Gas-phase infrared spectra in the range of 4200–550 cm^{-1} were recorded with a 2 cm^{-1} resolution from 32 co-added interferograms using a FTIR instrument (Bruker IFS 28).

(b) Mass Spectrometry. In order to perform mass spectra measurements, the reactor was connected directly to a FINNIGAN 3300 F-100 spectrometer and around 5 μmol of sample were injected. Spectra were obtained in the electron impact mode (EI) with 60 eV ionization energy.

(c) Computational details. First principles calculations were carried out using the MP2 and B3LYP methods in combination with different bases sets. They are specified in the First Principle Calculation section for each system. The highly accurate energy method Gaussian-2 (G2)[20] was used for the calculation of thermodynamic properties. All calculations were run with the Gaussian 09 program package.[21]

Results

Thermal decomposition was evaluated at 17 different temperatures (30 - 96 °C) using either N_2, O_2 or CO as bath gases and total pressures of 700 mbar. The measurements included an experimental run carried out in the absence of diluent gas. No discernible effect of either total pressure or nature of the diluent gas was observed on the decomposition rate. As stated before, the disappearance of the reagent was followed using its absorption bands at 1834 and 1907 cm^{-1}. The data were analyzed according to first-order kinetics:

$$-\frac{d[CH3_3OC(O)OOC(O)F]}{dt} = k_{exp}[CH_3OC(O)OOC(O)F] \qquad (3)$$

Figure 1 shows a plot of the logarithm of absorbance versus time for reactant loss with CO as diluent (plots for N_2 and O_2 as diluents are similar). Good straight lines were obtained in all cases. At each temperature studied, the first order rate constant was calculated from the plot by a least-squares method. Average rate constants are given in Table 1 along with the values obtained for N_2 and O_2 as diluent gases.

The collection of the rate constants for each bath gas as a function of temperature resulted in the following expressions

$$k_{exp,N_2}[CH_3OC(O)OOC(O)F] = (3.4 \pm 0.2)x\ 10^{14}\ s^{-1}\ \exp\left[-\frac{26.8 \pm 1.1\ kcal\ mol^{-1}}{RT}\right] \qquad (4)$$

$$k_{exp,O_2}[CH_3OC(O)OOC(O)F] = (7.6 \pm 0.3)x10^{14}s^{-1}\exp\left[\frac{-27.3 \pm 0.8 kcal mol^{-1}}{RT}\right] \qquad (5)$$

$$k_{exp,CO}[CH_3OC(O)OOC(O)F] = (8.4 \pm 0.2)x10^{14}s^{-1}\exp\left[\frac{-27.4 \pm 0.7 kcal mol^{-1}}{RT}\right] \qquad (6)$$

Plotting all the rate constants in a common Arrhenius plot (figure 2), it is clear that there is no particular dependence on either the nature or the pressure of the bath gas. Thus, the global expression for the rate constant obtained is $k_{exp} = (5.4 \pm 0.2) \times 10^{14}\ s^{-1} \exp[-(27.1 \pm 0.6\ kcal\ mol^{-1}/RT)]$.

Figure 3 shows the IR spectra of the reagent (red trace, A) and the products when the reaction is carried out with N_2 (blue trace, B) or CO (black trace, C) as bath gases. Traces B and C were obtained at the end of the reaction after the reagent had completely disappeared. As it can be seen in the figure, when N_2 is the bath gas $CH_3OC(O)OOC(O)F$ decomposition results in the formation of HF (from 3700 to 4200 cm^{-1}), CO_2 (2300 cm^{-1}), $CH_3OC(O)H$ (1960, 1750 and 1200 cm^{-1}), and smaller quantities of CO (773 cm^{-1}). The same products were obtained when the reaction was carried out with O_2 as bath gas. When using CO an additional product –$CH_3OC(O)F$– was formed.

Mass spectrometry was employed for further analysis of the products. The most important ions to consider are those with $m/z = 44$ and $m/z = 59$, which can be straightforwardly assigned to CO_2^+ and $CH_3OC(O)H^+$. The ratio of these signals yields a value of $CO_2/CH_3OCOH = 3.63$. This indicates that roughly four CO_2 molecules are generated for every $CH_3OC(O)H$ molecule. Traces (~1%) of CH_2O and HC(O)OH were found, which is in agreement with previous works,[11] though they were not detected by FTIR spectroscopy.

Discussion

Since the rate constants were independent of total pressure, it is assumed that these data are in the high pressure region, as expected for such a complex molecule. Examples of species that achieve their first-order values at low pressures are CF_3OOOCF_3,[14] $(CH_3C(O)O)_2$,[22] and $CH_3C(O)OONO_2$.[23]

The derived activation energy is 27.1 kcal mol^{-1}, and the extrapolated A factor is $10^{14.7}$, thus giving an activation entropy of 6.5 eu. The measured Arrhenius parameters are entirely reasonable for

the homogeneous gas phase decomposition of a large molecule into two smaller free radical fragments. The decomposition mechanism of diacyl peroxides is a topic of controversy. Formerly, three different paths were postulated: (1) a single peroxide bond cleavage to produce two carboxy radicals; (2) a stepwise pathway with two steps, the first one being the concerted rupture of bonds R—C(O)O—OC(O)R followed by decarboxylation of the carboxyl radical; and (3) the concerted bond cleavage of the three bonds R—C(O)O—OC(O)—R.[24] Nowadays only paths (1) and (2) remain accepted. The first one involves the O—O bond cleavage followed by subsequent decarboxylation of the RCO_2• radical. In the concerted one, two bonds simultaneously cleave yielding R•, CO_2, and •OR. Bartlett and coworkers suggested that concerted two-bond cleavage occurs whenever a sufficiently stable radical R• is formed [25,18]. In the last years, Schwarzer and collaborators have studied the photodecomposition of dibenzoyl peroxide[17] and tert-butyl-9-methylfluorene9-percarboxylate using femtosecond laser techniques[18]. Their experiments are consistent with a concerted O—O and phenyl—C(carbonyl) bond breakage. Supercritical fluids provide tunable solvent properties that are excellent candidates to examine the effect that both solvent cage and the transition from condensed to gas phase have on the decomposition reactions. DeSimone and collaborators[26] have used this approach to study the decomposition of bis(perfluoro-2-N-propoxypropionyl) peroxide (BPPP), trifluoro acetyl peroxide (TFAP), and acetyl peroxide (AP) and their results suggest a single bond O—O decomposition (stepwise mechanism). A theoretical investigation on the decomposition of diacyl peroxides in the gas phase[25] indicates that for diethyl peroxydicarbonate (DEPDC) and AP the concerted and stepwise mechanisms are likely to have similar activation energies while for TFAP the two-bond cleavage is the only pathway. This last assertion is supported by experiments and a sound interpretation of the mechanism given by Kopitzky and collaborators[27]. Moreover, thermal decomposition of linear diacyl peroxides like AP, BPPP, and $CF_3OC(O)OOC(O)OCF_3$ has also been explained in terms of the stepwise mechanism, so we could

reasonably expect the decomposition of $CH_3OC(O)OOC(O)F$ to be initiated by cleavage of the O-O bond.

Zhao has demonstrated that fluorination dramatically increases the decomposition kinetics of diacyl peroxides in the condensed phase because of the lowering of around 5-8 kcal mol-1in the activation enthalpies[28]. This tendency was supported by MNDO calculations[29] showing that the fluorine atom introduced at the α carbon makes the peroxy O—O bond longer and the dihedral angle C—O—O—C larger. This assertion is contradicted by more accurate calculations (using ab-initio methods[25]) which give, for instance , an activation energy for AP that is practically the same as the one for TFAP. Also, disagreement between calculated activation enthalpies (which mimic gas phase reactions) and experimental ones (taken from condensed phase decomposition) is larger than 5 kcal mol^{-1}. Gas phase activation energies and pre-exponential factors of closely related peroxides are presented in Table 2, where it can be observed that the fluorinated species have slightly larger activation energy than the hydrogenated ones. The discrepancy between gas and condensed phase behavior is not straightforward and suggests that the dynamics of the decomposition is indeed influenced by the solvent (the gas phase activation enthalpy for TFA differs by 7.4 kcal mol^{-1} from that measured with supercritical CO_2 as solvent).

The slight stabilization of fluorinated peroxides can be explained in terms of molecular orbitals. Levy et al. have described the R—O bond in ROOR considering electron donation from R to a π^* antibonding orbital of oxygen which contains an electron from oxygen.[30] This is the reason why the peroxidic bond in the FOOF molecule is shorter than in HOOH. Highly electronegative groups such as $–CF_3$ takes electron density from the antibonding orbital, while a group like $–CH_3$ donates electron density. The O—O bond would therefore be stronger in the former case.

$CH_3OC(O)OOC(O)F$ Decomposition Mechanism.

We present the mechanism for pyrolysis of the peroxide, which accounts for the products obtained. The first step in the decomposition process is the breaking of the peroxide bond, which is the weakest in the molecule.

$$CH_3OC(O)OOC(O)F \rightarrow CH_3OCO_2\bullet + FCO_2\bullet \quad (7)$$

Both radicals are susceptible to decarboxylation. Half-life, $t_{1/2}$, for FCO_2 has been reported to be of approximately 3 s at room temperature,[31] while the rate constant of the $CH_3OCO_2\bullet$ decomposition has not been measured so far. Because of this, it was assumed to be similar to the $CH_3CO_2\bullet$ radical (k = $5{,}14.10^8$ s^{-1})[32] giving a half-life of approximately 10^{-9} s. Thus, the next step in the mechanism is decarboxylation of the $CH_3OCO_2\bullet$ radicals

$$CH_3OCO_2\bullet \rightarrow CH_3O\bullet + CO_2 \quad (8)$$

which is much faster than the decarboxylation of $FCO_2\bullet$.

$$FCO_2\bullet \rightarrow F\bullet + CO_2 \quad (9)$$

Within the temperature range studied in this work, k_8 should leave no chance for reaction -7 to occur. We therefore conclude that the rate limiting step in the mechanism must be reaction 7, which all the parameters measured in the present contribution correspond to.

When using N_2 or O_2 as diluent, the products observed are $CH_3OC(O)H$ and HF (Figure 3). The appearance of the former could be explained through the following set of reactions

$$CH_3O\bullet + FCO_2\bullet \rightarrow CH_2O + HF + CO_2 \quad (10)$$

$$CH_2O + FCO_2\bullet \rightarrow CHO\bullet + HF + CO_2 \quad (11)$$

$$CH_3O\bullet + HCO\bullet \rightarrow CH_3OC(O)H \quad (12)$$

Reaction (10) should be expected to go through a recombination intermediate, either $CH_3OC(O)OF$, $CH_3OOC(O)F$ or both. Nevertheless a very simple sketch of both shows the possibility of the F atom

getting too close to one of the H atoms, thus opening the exit channel to give the products of reaction (10), because of thermodynamic control. In turn, the CH_2O formed is the required input to the formation of formyl radicals (CHO•), which by recombination with CH_3O• give the observed product.

The small amount of CO found could be formed by the reaction between HCO• and either FCO_2• or F• radicals, or by the recombination of two HCO• radicals

$$HCO• + F• \rightarrow HF + CO \quad (13)$$

$$HCO• + HCO• \rightarrow CH_2O + CO \quad (14)$$

When CO was used as bath gas, $CH_3OC(O)F$ was observed in addition to the products found with N_2. Reactions 10 to 12 certainly occur in this system, but CO can also react with both CH_3O• radicals and F• atoms to form $CH_3OC(O)$• and FCO•, respectively[33,34].

$$CH_3O• + CO \rightarrow CH_3OCO• \quad (15)$$

$$F• + CO \rightarrow FCO• \quad (16)$$

The new product observed is formed by recombination of $CH_3OC(O)$• with F / FCO• and CH_3O• with FCO•.

$$CH_3OC(O)• + F / FCO• \rightarrow CH_3OC(O)F \ /+ \ CO \quad (17)$$

$$CH_3O• + FCO• \rightarrow CH_3OC(O)F \quad (18)$$

On account of the mechanism just outlined, a simulation of the temporal progression of the reaction was carried out using the Kintecus[35] program which was fed with literature rate constants for all reactions but reaction 7 where our parameters were used. The result of such a simulation is represented in Figure 4 by the solid lines. Superimposing our experimental results, taken from IR absorptions, a perfect match between them is clearly observed, thus giving support to our mechanism. Besides, an interesting comparison can be made with the results obtained from the mass spectrum as well as from

IR measurements. The ratio between CO_2 and $CH_3OC(O)H$ is again around 4. This is a strong evidence for the occurrence of reactions (10-12) in the way they are written.

First Principle Calculations

Transition States. The strength of the O—O bond in hydrogenated dialkyl peroxides has usually been measured as about 37 kcal mol^{-1} and it is rather independent of the alkyl group. The experimental O—O bond energy for diacyl peroxides was estimated to be around 30 kcal mol^{-1}. Theoretical calculations correctly predict bond dissociation only for alkyl peroxides, while for acyl ones, the values were believed to be strongly overestimated.[15,25,36,37]. State of the art ab initio calculations like post CCSD(T) are used to evaluate different molecular properties of peroxides[38] although to the best of our knowledge, reference [25] presents the last theoretical investigation concerning the decomposition of diacyl peroxides. Using MP2 and DFT calculations several TS were explored for the two different dissociation pathways obtaining activation energies of 44, 30, and 27 kcal mol-1 for DEPDC, AP, and TFA respectively. Schlegel et al. proposed that the dissociation process is far more complex than a simple homolytic cleavage of the O—O bond,[15] based on the mechanism involving a scrambling intermediate (or transition state) that could explain the low activation energy found experimentally for diacyl peroxides.[39,40] Fujimori and collaborators also used DFT calculations to study thermal reorganization of diacyl peroxides suggesting that oxygen scrambling in diacyl peroxides occurs via a σ-acyloxyl radical pair.[37]

The simple bond decomposition process for $CH_3OC(O)OOC(O)F$ was evaluated at G2 and UB3LYP/6-31++G(d,p) levels as the energy difference of reactant and the fragments CH_3OCO_2/FCO_2 separated by 5 Å. For the DFT calculation, thermal energies including ZPE were evaluated from the vibrational frequencies at the optimized structures using tight convergence cutoff criteria. Mixing of the

HOMO/LUMO molecular orbitals was employed, despite the unavoidable spin contamination introduced, in order to obtain better solutions in terms of the energies involved. The energies so obtained were 39 and 18 kcal mol^{-1} for the G2 and UB3LYP methods respectively. The difference of 21 kcal mol^{-1} between both methods could be probably due to the failure of DFT to accurately describe the transitions state involved, since it is not uncommon the underestimation of the barrier for these type of processes. The energy difference for the dissociation process that yields $CH_3O•$, CO_2, and $FCO_2•$ lowers the energy to 29 and 10 kcal mol^{-1} for G2 and UB3LYP respectively due to exothermic decarboxylation of $CH_3CO_2•$. In this case, the energy of the G2 method is very close to the experimental one (27 kcal mol^{-1}) and this can be thought of as an indication that the G2 potential energy surface (PES) favors a concerted CH_3O—C(O)O—OC(O)F bond cleavage with a loose TS similar to products.

A relaxed PES scan of the O—O bond distance from 1 to 5 Å using the UB3LYP method, was run with tight convergence optimizations. The calculations converged normally for points with O—O bond distances shorter than 1.8 Å and larger than 3.3 Å indicating a complex PES with saddle points for distances of around 2 Å. Eight possible transition states were calculated to represent these points in the reaction coordinate. Some of the energy differences observed between them amounted to 40 kcal mol^{-1} indicating a hilly PES. The two lowest energy TS found are almost equivalent conformers (SP-RingSyn and SP-RingAnti) differing in 0,9 kcal mol^{-1} with 28 kcal mol^{-1} above the minimum geometry of $CH_3OC(O)OOC(O)F$, figure 5 shows the structures. The activation energy obtained is in good agreement with the experimental one. The structure of these two TS corresponds to the planarization of the C—O—O—C dihedral until a quasi-symmetric cyclic diperoxide structure is reached. This agrees with the σ acyloxyl radical pair suggested by Fujimori in the scrambling reaction of formyl peroxide[37]. From any of these scrambled TS, a synchronic lengthening of the diperoxide bonds conducts to the

formation of FCO_2 and CH_3OCO_2 radicals. Further decomposition and reactions of these radicals fully conform to the proposed mechanism.

Another interesting point about this transition state is that the entropy found by calculations is 7,7 eu, very similar to that inferred from the measurements (6,5 e.u., see Table 2). It is usually accepted that the activation entropy for a concerted reaction is negative. However, that is not the case here, as calculations and experiments show, because the transition state is a very loose one with substantially long O—O bond lengths.

CH_3OCO_2• Radical. Though acyloxy radicals are involved in almost any degradation reaction from carbonylic compounds occurring in the atmosphere,[41-43] and the considerable effort devoted to the study of hydrofluorinated radicals,[44-46] it is surprising that CH_3OCO_2•, one of the simplest hydrogenated acyloxy radicals has received so little attention. It is difficult to obtain experimental spectroscopic and thermochemical properties for short-lived species, and thus theoretical models have become a proper tool for their investigation and prediction. In the next paragraphs, we provide geometrical parameters, vibrational frequencies, and heats of formation by using different ab initio methods.

Geometrical Parameters. At first glance, there are two different possibilities for the conformation of the acyloxy radical, both comprising the *Cs* symmetry group. The plane formed by the —CO_2 moiety could be parallel (A) or perpendicular (B) to the C-O-C-H chain. However, calculations starting with B geometry always converge to A. The geometry obtained through the B3LYP/6-311++G** method is presented in Figure 6, where atom labeling is used to identify the different geometrical parameters, which are shown in Table 3 for the different methods studied. From the analysis, it appears that the radical does not share equally the unlocalized electrons, since the O1—C2 bond shows a distance which is shorter than that for a simple bond giving the idea of a quasi-double bond which will hinder

the free rotation of the CO_2 group. This allows the O2 atom to interact with the hydrogen atoms of the CH_3 group thus reinforcing the O2—C2 bond. This is also seen through the difference in distances C2—O2 and C2—O3 since the former is shorter. A simple calculation of the energy required for the rotation of the CO_2 group shows that it is a process requiring an activation energy larger than for a true simple bond (calculated 7 kcal mol^{-1}).

The MP2 method gives longer distances for the O—C bonds and emphasize the differences in the O2—C2 and C2—O3 bond lengths. Also the bond angles are calculated wider.

Vibrational Analysis. The vibrational frequencies for the CH_3OCO_2• radical obtained at the MP2/6-311++G** and DFT-B3LYP/6-311++G** level of theory are presented in Table 4.

Assuming that the point group for the CH_3OCO_2• radical is *Cs*, all 18 fundamental modes should be both IR and Raman active, twelve of them belonging to A´ representation and six to A´´. All the vibrational frequencies are real and positive. The frequencies and intensities obtained with both methods shows remarkable differences, mainly in those vibrations involving the CO_2 fragment. In general MP2 frequencies are higher with the exception of ν8. These differences can be explained in terms of the way that each method takes into account the —CO_2 delocalization, being the B3LYP the one that distributes more evenly the resonant effect. The ν_3 mode, assigned to a C=O stretch appears at 1806 and 1577 cm^{-1} at the MP2 and B3LYP methods, respectively. The former understands the movement as a pure C=O stretch while for the second, the mode is coupled and involves more atoms in the movement. Because of this effect, the mode shown in the table cannot be unambiguously assigned to a pure stretching. The assigned shown in the last column of the table was done from the evaluation of the normal modes displacement vectors; as many of the modes are strongly coupled this information is rather subjective.

Heat of Formation. In order to get insight into the thermodynamic properties of this radical, its heat of formation was obtained by mean of three approaches (isodesmic, atomization and formation reactions) at the G2 level, using in all cases the lower energy structures.

The first approach is based on a series of isodesmic reactions (19-22), shown in Table 5. In this type of reactions the reactants and products contain the same type and number of bonds. Because of the electronic similarity, errors due to limitation in the basis set, electron correlation energy and spin contamination nearly cancel between reactants and products. The reaction enthalpies and the heat of formation $\Delta H°_{f\,298}(CH_3OCO_2•)$ computed at 298 K are informed in the table as well. The following experimental values[47] were used for the evaluation of $\Delta H°_{f\,298}(CH_3OCO_2•)$: CH_3CH_3 (–20.04 ± 0.07), $CH_3C(O)O•$ (–46.0), CH_3OCH_3 (-44.0 ± 0.1), CO (–26.42 ± 0.04), CH_2O (–25.98 ± 0.01), CH_3OH (-48.1 ± 0.1), CO_2 (–94.05 ± 0.03), OH• (8.89 ± 0.09), $CH_3•$ (35.05±0.07) and $CH_3OCO•$ (−37 ± 3),[44] all in units of kcal mol^{-1}. The enthalpy of formation for the radical, obtained as the average value from reactions (19-22) is $\Delta H°_{f\,298}(CH_3OCO_2•)$ = (-79 ± 3) kcal mol^{-1}. The uncertainty informed takes into account the broad dispersion found in the literature.

The second and third approaches involve the atomization reaction (23) and the combustion reaction (24) of table 5. These have been used by Bérces et al. as suitable methods for the calculation of thermodynamic properties of hydrogenated radicals.[48] Using reaction (23) and the heat of formation at 298K of the species O (59.56 ± 0.02), H (52.103 ± 0.001) and C (171.3 ± 0.1), the value of $\Delta H°_{f\,298}(CH_3OCO_2•)$ = (-74,8 ± 0,1) kcal mol^{-1} is obtained. When using reaction (24) of the table and the enthalpies of formation of H_2, O_2 and C, the calculated value is $\Delta H°_{f\,298}$ $(CH_3OCO_2•)$ = (-79,8 ± 0.1) kcal mol^{-1}.

Taking the average of the values obtained with the three methods, the suggested heat of formation for the radical is $\Delta H°_{f\,298}$ $(CH_3OCO_2•)$ = (-78 ± 3) kcal mol^{-1}. It is interesting to note that this value along

with $\Delta H°_{f\,298}$ ($CH_3O•$) = -4.1 ± 0.9 kcal mol^{-1} and $\Delta H°_{f\,298}$ (CO_2) = -94.14 kcal mol^{-1} leads to a reaction enthalpy of -20 kcal mol^{-1} for $CH_3OCO_2• \rightarrow CH_3O• + CO_2$.

We have listed in Table 6 the enthalpy values for some related decarboxylation reactions. As it can be seen, for the first three radicals, the enthalpy is informed as well as their lifetimes for decarboxylation. A brief comparison shows that the lifetimes shorten as the reaction becomes less endothermic and continue to do so when it becomes exothermic. This could be rationalized in terms of a thermodynamic control of the reaction rate. Within this approach, the lifetime for the $CH_3OCO_2•$ radical would become extremely small, giving support to our former conclusion that reaction (8) should be very fast.

Heat of Formation of $CH_3OC(O)OOC(O)F$. The heat of formation of $CH_3OC(O)OOC(O)F$ was derived from the rate constant for decomposition by performing second law calculations. Within this approach, the heat of formation is obtained from the Arrhenius activation energy, which provides the heat of reaction as $\Delta_r H° = Ea - RT$.

For $CH_3OC(O)OOC(O)F$, $\Delta H°_r$ = 26.5 kcal mol^{-1}. Therefore, $\Delta H°_{f\,298}$ is obtained from the expression

$$\Delta H^o_{f\,298}(CH_3OC(O)OOC(O)F) = \Delta H^o_{f\,298}(CH_3OCO_2^•) + \Delta H^o_{f\,298}(FCO_2^•) - \Delta H^o_r$$

with our value for $\Delta H°_{f\,298}$ ($CH_3OCO_2•$) of -78 ± 3 kcal mol^{-1} and the value for $\Delta H°_{f\,298}$ ($FCO_2•$) as -87 ± 2 kcal mol^{-1}.[51] The heat of formation of $CH_3OC(O)OOC(O)F$ is $\Delta H°_{f\,298}$ = - 191 ± 5 kcal mol^{-1}.

A second evaluation of the heat of formation was carried out with the isodesmic approach at G2 level using reactions 26 and 27 where all the species involved are well known.

$CH_3OC(O)OOC(O)F + 2\ CH_3• \rightarrow CH_3OOCH_3 + FCO• + CH_3OC(O)•$ (26)

$CH_3OC(O)OOC(O)F + CF_3O• \rightarrow CF_3OC(O)OOC(O)F + CH_3O•$ (27)

Though reactions 26 and 27 include radicals, the computed values of $\Delta H°_{f\,298}$ ($CH_3OC(O)OOC(O)F$) were 200 and 191 kcal mol^{-1} respectively in excellent agreement with our experimental value.

Conclusion

In the present paper the gas phase thermal decomposition of $CH_3OC(O)OOC(O)F$ has been studied for temperatures between 303 and 371 K. The decomposition proceeds with first order kinetics and the activation energy amounts to 27.1 kcal mol^{-1}. The calculations run agreed with the experimental values and showed a mechanism were the transition state involves a scrambling geometry. Comparison of our values with other related peroxides shows that fluorination does not dramatically change the activation energies for dissociation as opposed to what is observed in condensed media.

ACKNOWLEDGMENTS Financial support from Consejo Nacional de Investigaciones Científicas y Técnicas (CONICET), FONCyT, and SECyT-UNC is gratefully acknowledged. M.B. is indebted to CONICET for funding his Ph.D studies.

Figure 1. First-order decomposition of $CH_3OC(O)OOC(O)F$ in CO as diluent.

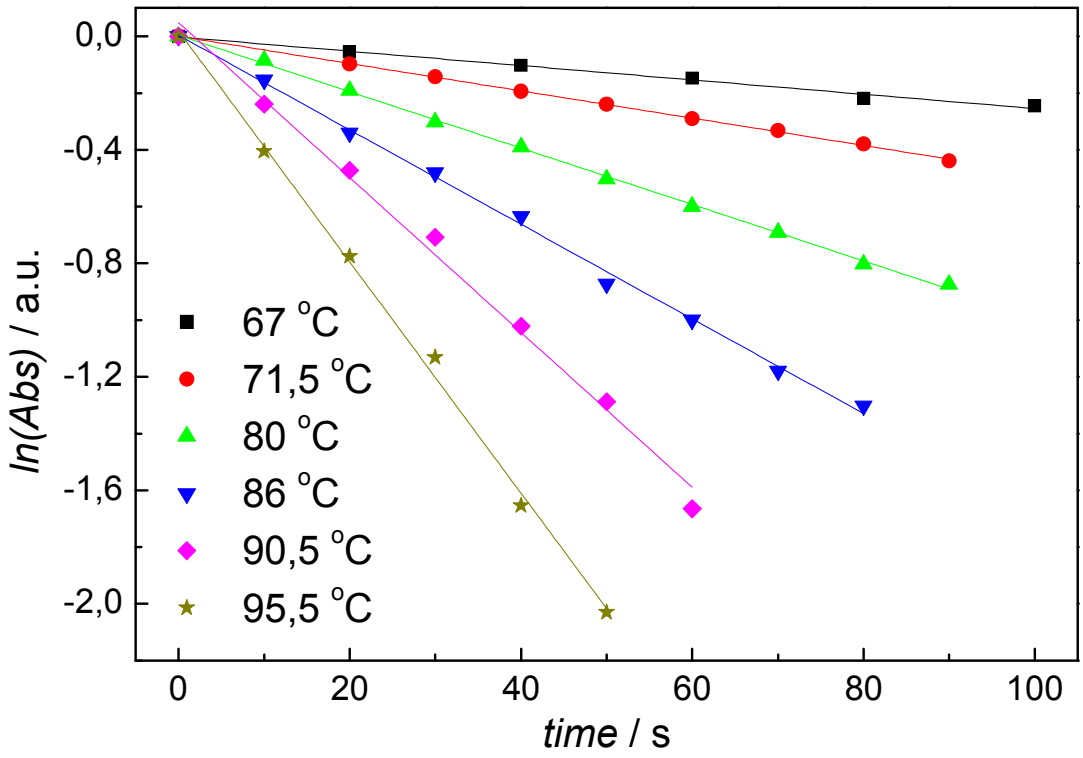

Figure 2. Arrhenius plot for the decomposition of $CH_3OC(O)OOC(O)F$ in N_2, O_2 and CO diluents.

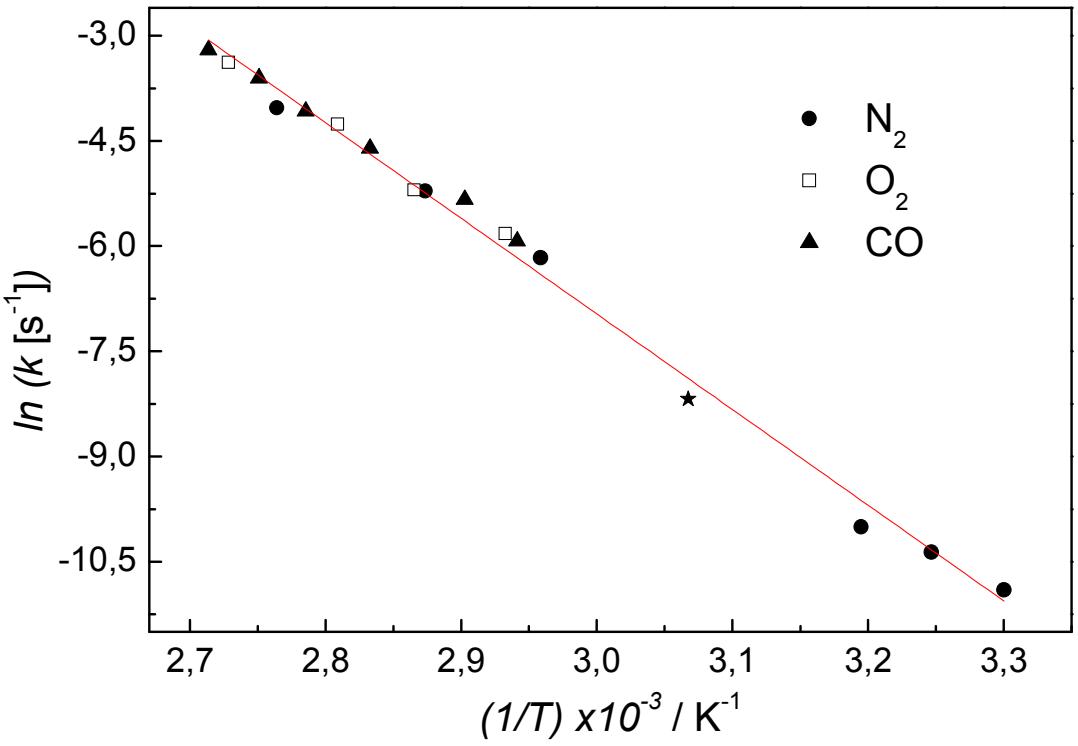

Figure 3. IR spectra of $CH_3OC(O)OOC(O)F$ (red trace) and their decomposition products in N_2 (blue trace, KBr windows used) and CO (black trace, sapphire windows) as diluents.

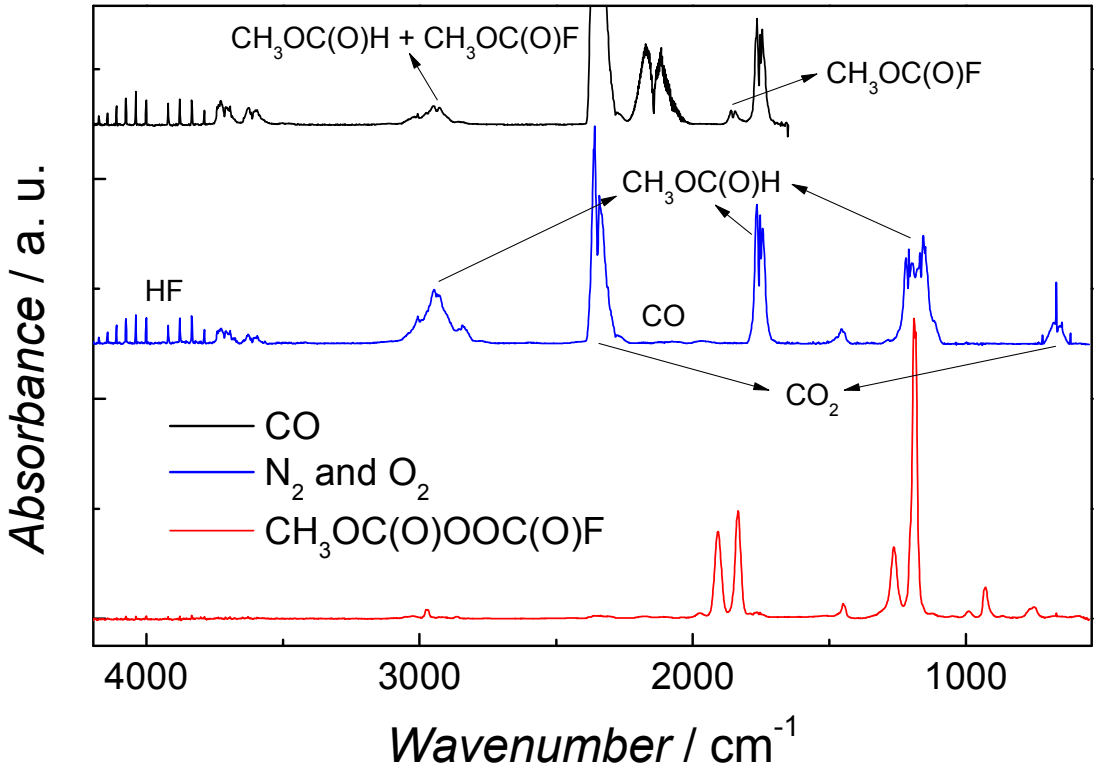

Figure 4. Calculated and experimental concentration–time profiles. Solid lines represent the output of the kinetic simulation for a temperature of 35 ºC using N_2 as bath gas. Superimposed symbols correspond to experimental data points. ■ $CH_3OC(O)OOC(O)F$; ● $CH_3OC(O)H$; ♦ CO_2; ▲ CH_2O.

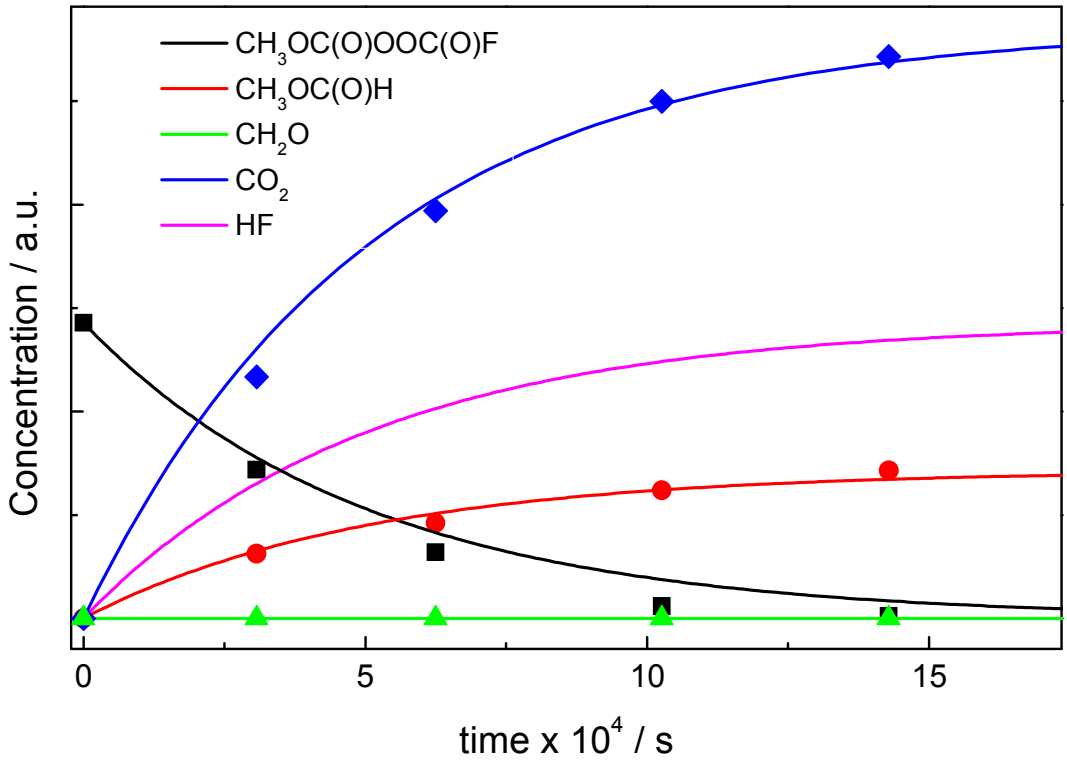

Figure 5. Calculated structures of the transition states at the B3LYP/6-31++G**

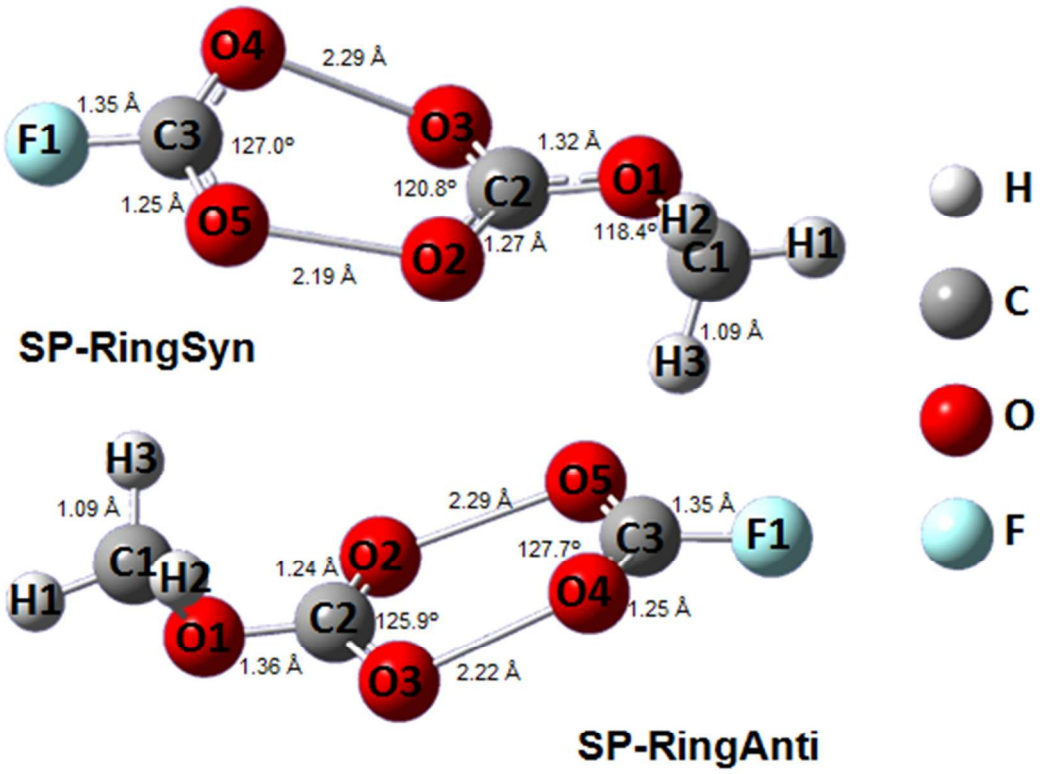

Figure 6. Calculated structure (B3LYP/6-311++G**) of the CH_3OCO_2• radical.

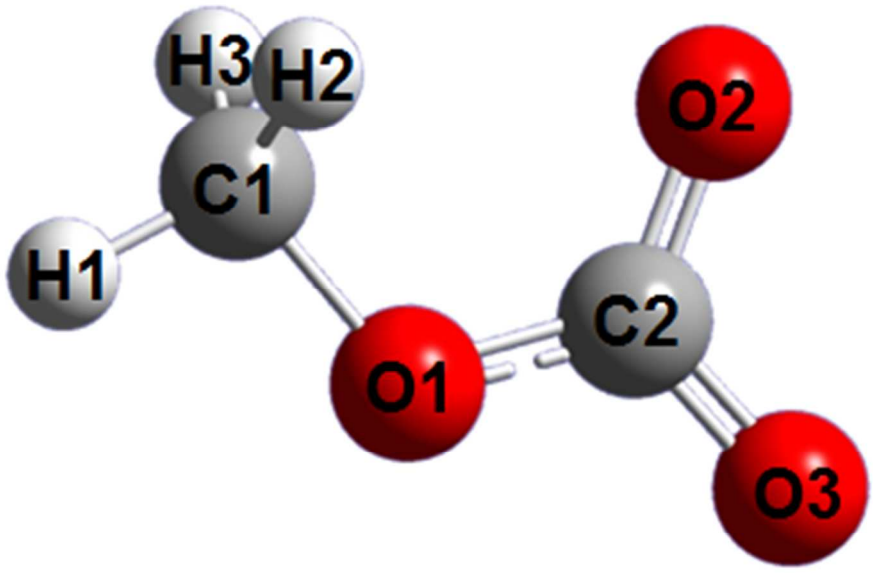

Table 1. First-Order Decomposition Rate Constants of $CH_3OC(O)OOC(O)F$ (s^{-1}) at different temperatures (ºC) for each bath gas.

Bath gas					
N_2		O_2		CO	
T	*k*	*T*	*k*	*T*	*k*
30	$(1.84 \pm 0.10) \times 10^{-5}$	68	$(2.96 \pm 0.10) \times 10^{-3}$	67	$(2.66 \pm 0.06) \times 10^{-3}$
35	$(3.15 \pm 0.22) \times 10^{-5}$	76	$(5.52 \pm 0.04) \times 10^{-3}$	71.5	$(4.81 \pm 0.05) \times 10^{-3}$
40	$(4.52 \pm 0.30) \times 10^{-5}$	83	$(1.41 \pm 0.03) \times 10^{-2}$	80	$(9.99 \pm 0.11) \times 10^{-3}$
53	$(2.80 \pm 0.07) \times 10^{-4}$	93.5	$(3.40 \pm 0.06) \times 10^{-2}$	86	$(1.70 \pm 0.03) \times 10^{-2}$
65	$(2.10 \pm 0.06) \times 10^{-3}$			90.5	$(2.73 \pm 0.10) \times 10^{-2}$
75	$(5.46 \pm 0.18) \times 10^{-3}$			95.5	$(4.07 \pm 0.11) \times 10^{-2}$
88,8	$(1.78 \pm 0.01) \times 10^{-2}$				

Table 2. Activacion Energy, Pre-exponential Factors, Enthalpy and Entropy of Activation for Selected Molecules. [a] CO_2 solvent.

Compound	Activation Energy (kcal mol^{-1})	A	$\Delta H^{\#}$ (kcal mol^{-1})	$\Delta S^{\#}$ (eu)	Ref.
$CH_3OC(O)OOC(O)F$	27.1	$10^{14.7}$	24.3	6.5	This work
$CF_3OC(O)OOC(O)F$	29.0	$10^{15.6}$	26.1	10.5	[12]
$CH_3C(O)OOC(O)CH_3$	29.5	$10^{14.2}$	28.8	4.3	[22]
$CF_3C(O)OOC(O)CF_3$	30.9	$10^{15.3}$	28.2 20.8	9.4 -14.1	[27] [26] [a]

Table 3. Ab Initio Geometrical Parameters of the CH_3OCO_2• Radical.

	DFT / B3LYP		MP2
	6-31G	6-311++G**	6-311++G**
Bond Lengths (Å)			
O(3)-C(2)	1.296	1.263	1.337
O(2)-C(2)	1.273	1.244	1.205
C(2)-O(1)	1.344	1.318	1.331
O(1)-C(1)	1.483	1.451	1.444
C(1)-H(2)	1.091	1.090	1.090
C(1)-H(1)	1.087	1.086	1.087
C(1)-H(3)	1.091	1.090	1.090
Bond Angles (deg)			
O(3)-C(2)-O(2)	116.41	115.38	121.74
C(2)-O(1)-C(1)	117.54	116.76	113.63
O(1)-C(1)-H(1)	104.08	104.83	104.87
H(2)-C(1)-H(3)	110.44	110.23	110.13
O(2)-C(2)-O(1)-C(1)	0.000	0.00000	0.000
O(3)-C(2)-O(1)-C(1)	-180.000	-180.00000	-180.000
C(2)-O(1)-C(1)-H(1)	179.998	179.999	179.997

Table 4. Vibrational frequencies (cm^{-1}) and intensities for the CH_3OCO_2• radical calculated using the 6-311++G(d,p) basis set.

Mode Symm.	Mode	Frequencies		Intensities		Mode description
		MP2	B3LYP	MP2	B3LYP	
A’	ν_1	3240	3174	6,14	5,32	CH_3 asym. stretch
	ν_2	3110	3059	20,72	15,92	CH_3 sym. stretch
	ν_3	1807	1577	363,57	467,42	CO stretch
	ν_4	1524	1496	9,06	17,94	CH_3 deformation
	ν_5	1501	1449	18,81	92,39	CH_3 umbrella
	ν_6	1343	1225	501,72	44,62	H-C-O’ bend
	ν_7	1233	1194	18,05	36,25	H-C-O bend
	ν_8	1091	1095	29,21	99,92	C-O-C asym. stretch
	ν_9	916	906	34,05	6,23	COC sym. stretch
	ν_{10}	648	628	0,28	1,92	OCO bend
	ν_{11}	452	507	24,00	29,96	OCO’ bend
	ν_{12}	284	259	6,98	4,90	COC bend
A’’	ν_{13}	3209	3139	11,44	12,26	CH_3 asym. stretch
	ν_{14}	1508	1488	9,21	11,57	CH_3 deformation
	ν_{15}	1196	1169	1,15	0,60	CH_3 twist
	ν_{16}	774	760	25,86	36,24	COCO torsion
	ν_{17}	158	148	2,53	2,18	HCOC torsion
	ν_{18}	122	92	1,43	0,05	H_3COC torsion

Table 5. Isodesmic, Atomization and Pseudo-Formation Reactions used for the calculation of the heat of formation of the radical CH_3OCO_2• at G2 level of theory.

Reaction	ΔH_r (kcal mol^{-1})	ΔH_f (CH_3OCO_2•) (kcal mol^{-1})	
CH_3OCO_2• + CH_3CH_3 → $CH_3C(O)O$• + CH_3OCH_3	11.64	-80.60	-78.82
CH_3OCO_2• + CO → CH_3OCO• + CO_2	-26.49	-78.45	
CH_3OCO_2• + CH_3OH → CH_3OCH_3 + CO_2 + OH•	-3.22	-77.90	
CH_3OCO_2• + CH_3• → CH_3OCH_3 + CO_2	-94.78	-78.32	
CH_3OCO_2 → 3 H + 2 C + 3 O	-752.34	-74.79	
2 C + 3/2 O_2 + 3/2 H_2 → CH_3OCO_2•	-422.41	-79.83	
Mean		-77.81	

Table 6. Heat of reaction for the decarboxylation $R—CO_2• \rightarrow R• + CO_2$. Lifetime of some species is also presented.

Name	ΔH^o_r	Lifetime (s)	Ref.
$F—CO_2•$	11	3	[13]
$CF_3—CO_2•$	4.9	10^{-4}	This Work,[13]
$CH_3—CO_2•$	-13	10^{-9}	[49,50]
$CF_3O—CO_2•$	-14		[13]
$CH_3O—CO_2•$	-20		This Work

REFERENCES

(1) Calvert, J.; Mellouki, A.; Orlando, J.; Pilling, M.; Wallington, T. Mechanisms of Atmospheric Oxidation of the Oxygenates. Oxford University Press, New York, 2011 and references cited therein.

(2) Argüello, G. A.; Willner, H. *J. Phys. Chem. A.* 2001, *105*, 3466.

(3) von Ahsen, S.; Willner, H.; Francisco, J. S. *Chem. Eur. J.* **2002**, *8*, 4675.

(4) von Ahsen, S.; Hufen, J.; Willner, H.; Francisco, J. S. *Chem. Eur. J.* **2002**, *8*, 1189.

(5) Hohorst, F. A.; DesMarteau, D. D.; Anderson, L. R.; Gould, D. E.; Fox, W. B. *J. Am. Chem. Soc.* **1973**, *95*, 3866.

(6) Arvía, A. J.; Aymonino, P. J.; Schumacher, H. J. *An. Asoc. Quím. Argent.* **1962**, *50*, 135, 1195.

(7) Argüello,G. A.; Willner, H.; Malanca, F.E. Inorg. Chem.,**2000**, 39, 1195.

(8) Argüello, G. A.; von Ahsen, S.; Willner, H.; Burgos Paci, M. A.; García, P. *Chem. Eur. J.* **2003**, *9*, 5135.

(9) Burgos Paci, M. A.; García, P.; Malanca, F. E.; Argüello, G. A.; Willner, H. *Inorg. Chem.* **2003**, *42*, 2131.

(10) Pernice, H.; Berkey, M.; Henkel, G.; Willner, H.; Argüello, G. A.; McKee, M. L.; Webb, T. R. *Angew. Chem.* **2004**, *116*, 2903.

(11) Berasategui, M.; Burgos Paci, M. A.; Argüello, G.A. *Z. Anorg. Allg. Chem.* **2012**, *638*, 547.

(12) Burgos Paci, M. A.; Argüello, G. A.; García, P.; Willner, H. *Int. J. Chem. Kinet.* **2003**, *35*, 15.

(13) Burgos Paci, M. A.; Argüello, G. A.; García, P.; Willner, H. *J. Phys. Chem. A.* **2005**, *109*, 7481.

(14) Czarnowski, J.; Schumacher, H. J. *Int. J. Chem. Kinet.* **1981**, *13*, 639.

(15) Bach, R. D; Ayala, P. Y.; Schlegel H. B. *J. Am. Chem. Soc.* **1996,** *118*, 12758.

(16) Vennekate, H.; Walter, A.; Fischer, D.; Schroeder, J.; Schwarzer, D. Z. *Phys. Chem.* **2011**, *225*, 1089.

(17) Reichardt, C.; Schroeder, J.; Vohringer, P.; Schwarzer, D. *Phys. Chem. Chem. Phys*, **2008**, *10*, 1662.

(18) Reichardt, C.; Schroeder, J.; Schwarzer, D. *Phys. Chem. Chem. Phys*, **2008**, *10*, 5218.

(19) Buback, M.; Kling, M.; Schmatz, S; Schroeder, J. *Phys. Chem. Chem. Phys*, **2004***, 6*, 5441.

(20) Curtiss, L. A.; Raghavachari, K.; Trucks, G. W.; Pople, J. A. *J. Chem. Phys.* **1991**, 94, 7221.

(21) M. J. Frisch, G. W. Trucks, H. B. Schlegel, G. E. Scuseria, M. A. Robb, J. R. Cheeseman, G. Scalmani, V. Barone, B. Mennucci, G. A. Petersson, H. Nakatsuji, M. Caricato, X. Li, H. P. Hratchian, A. F. Izmaylov, J. Bloino, G. Zheng, J. L. Sonnenberg, M. Hada, M. Ehara, K. Toyota, R. Fukuda, J. Hasegawa, M. Ishida, T. Nakajima, Y. Honda, O. Kitao, H. Nakai, T. Vreven, J. A. Montgomery Jr., J. E. Peralta, F. Ogliaro, M. Bearpark, J. J. Heyd, E. Brothers, K. N. Kudin, V. N. Staroverov, R. Kobayashi, J. Normand, K. Raghavachari, A. Rendell, J. C. Burant, S. S. Iyengar, J. Tomasi, M. Cossi, N. Rega, J. M. Millam, M. Klene, J. E. Knox, J. B. Cross, V. Bakken, C. Adamo, J. Jaramillo, R. Gomperts, R. E. Stratmann, O. Yazyev, A. J. Austin, R. Cammi, C. Pomelli, J. W. Ochterski, R. L. Martin, K. Morokuma, V. G. Zakrzewski, G. A. Voth, P. Salvador, J. J. Dannenberg, S. Dapprich, A.

D. Daniels, O. Farkas, J. B. Foresman, J. V. Ortiz, J. Cioslowski, D. J. Fox, *Gaussian 03*, Gaussian, Inc., Wallingford CT, **2009**.

(22) Rembaum, A.; Szwarc, M. *J. Am. Chem. Soc.* **1954**, *76*, 5.

(23) Cox, R. A.; Roffey, M. J. *En*V*iron. Sci. Technol.* **1977**, *11* (9), 900.

(24)Fujimori, K. Diacyl Peroxides. *Organic Peroxides*, Ando, W., Ed.; Wiley: New York, **1992**; 319.

(25) Gu, Z; Wang, Y.; Balbuena, P.B. *J. Phys. Chem. A*. **2006**, *110*, 2448.

(26) Bunyard, W.C.; Kadla, J.F.; De Simone, J.M. *J. Am. Chem. Soc.* **2001**, *123*, 7199.

(27) Kopitzky, R.; Willner, H.; Hermann, A.; Oberhammer, H. *Inorg Chem* **2001**, *40*, 2693–2697.

(28) Zhao, C.; Zhou, R.; Pan, H.; Jin, X.; Qu, Y.; Wu, C.; Jiang, X. *J. Org. Chem.* **1982***, 47*, 2009.

(29) Sawada, H.; Nakayama, M.; Kikuchi, O.; Yocoyama, Y. *J. Fluor Chem.* **1990**, *50*, 393.

(30) Maricq, M. M.; Szente, J. J.; Khitrov, G. A.; Francisco, J. S. J. Chem. Phys. 1993, 98, 9522.

(31) Wallington, T. J.; Hurley, M. D.; Matti Maricq, M. *Chem. Phys. Lett.* **1993**, *205*, 63.

(32) Zhou, Y. Z.; Li, S.; Li, Q. S.; Zhang, S. W. *J. Mol. Struct.*, **2008**, *854*, 40.

(33) Wang, B.; Hou, H; Gu Y.*J. Phys. Chem. A*, **1999**, *103*, 8021.

(34) Arutyunov, V. S.; Buben, S. N.; Chaikin, A. M. *Kinet. Catal. Lett.*, **1975**, *3*, 205.

(35) J. C. Ianni, KINTECUS V 4.0.0.

(36) Bouillon, G.; Lick, C.; Shank, K. in *The Chemistry of Functional Groups Peroxides*; Patai, S., Ed.; John Wiley & Sons: New York, 1983; p 279

(37) Uchimaru, T.; Hara, R.; Tanabe, K; Fujimori, K. *Chem. Phys. Lett.* **1997**, *267*, 244

(38) Karton, A; Parthiban, S; Martin, J.M.L. *J. Phys. Chem. A* **2009**, *113,* 4802.

(39) Goldstein, M. J.; Judson, H. A. *J. Am. Chem. Soc.* **1970**, *92*, 4119.

(40) Goldstein, M. J.; Haiby, W. A. *J. Am. Chem. Soc.* **1974**, *96*, 7358.

(41) Hilborn, J. W.; Pincock, J. A. J. Am. Chem. Soc. 1991, 113, 2683.

(42) Rokhina, E. V.; Makarova, K.; Golovina, E. A.; Van As, H.; Virkutyte, J. *Environ. Sci. Technol.*, **2010**, 44, 6815.

(43) Peukert, S. L.; Sivaramakrishnan, R.; Michael, J. V. *J. Phys. Chem. A*, **2013**, 117, 3718.

(44) Francisco, J. S. *J. Chem. Phys.* **1998**, 237, 1.

(45) von Ahsen, S.; García, P.; Willner, H.; Argüello, G. A. *Inorg. Chem.*, 2005, 44, 5713.

(46) Burgos Paci, M. A.; Argüello, G. A. *Chem. Eur. J.*, **2004**, 10, 1838.

(47) Sander, S. P.; Friedl, R. R.; Golden, D. M.; Kurylo, M. J.; Huie, R. E.; Orkin, V. L.; Moortgat, G. K.; Ravishankara, A. R.; Kolb, C. E.; Molina, M. J.; Finlayson-Pitts, B. J. *Chemical kinetics and Photochemical Data for Use in Stratospheric Modeling. Evaluation 14, JPL Publ. 02-25,* **2003**.

(48) Viskolcz, B.; Bérces, T. *Phys. Chem. Chem. Phys.* **2000**, *2*, 5430.

(49) Zhou, Y.Z.; Li, S.; Li, Q.S.; Zhang, S.W. *J. Mol. Struct. Theochem.* **2008**, 854, 40.

(50) Miller, C. E.; Lynton, J. I.; Keevil, D. M.; Franscisco J. S. *J. Phys. Chem. A*, **1999**, 103, 11451.

(51) Dibble, T. S.; Francisco, J. S. *J. Phys. Chem.* **1994**, *98*, 11694.

Table of Content Image (TOC)